Tailoring compositionally graded interface of 316L stainless steel to Al12Si aluminum alloy bimetallic structures via Additive Manufacturing

Yanning Zhang and Amit Bandyopadhyay*

W. M. Keck Biomedical Materials Research Laboratory

School of Mechanical and Materials Engineering

Washington State University

Pullman, WA 99164-2920, USA.

*Corresponding author's E-mail: amitband@wsu.edu

Abstract

316L stainless steel (SS) to Al12Si aluminum alloy structures were processed, tailoring the compositionally graded interface on a SS 316 substrate using a directed energy deposition (DED)-based additive manufacturing (AM) process. Applying such a compositionally graded transition on bimetallic materials, especially joining two dissimilar metals, could avoid the mechanical property mismatch. This study's objective was to understand the processing parameters that influence the properties of AM processed SS 316L to Al12Si bimetallic structures. Two different approaches fabricated these bimetallic structures. The results showed no visible defects on the as-fabricated samples using 4 layers of Al-rich mixed composition as the transition section. The microstructural characterization showed a unique morphology in each section. Both cooling rate and compositional variations caused microstructural variation. FeAl, Fe_2Al_5, and $FeAl_3$ intermetallic phases were formed at the compositionally graded transition section. After stress relief heat-treatment of SS 316L/Al12Si bimetallic samples, diffused intermetallic phases were seen at the compositionally graded transition. At the interface, as processed, bimetallic structures had a microhardness value of 834.2 ± 107.1 $HV_{0.1}$, which is a result of the $FeAl_3$ phase at the compositionally graded transition area. After heat-treatment, the microhardness value reduced to 578.7 ± 154.1 $HV_{0.1}$ due to more Fe dominated Fe_xAl_y phase formation. The compression test results showed that the non-HT and HT SS 316L/Al12Si bimetallic structures had a similar maximum compressive strength of 299.4 ± 22.1 MPa and 270.1 ± 27.1 MPa, respectively.

Keywords: Directed-energy deposition; Bimetallic structures; SS 316; Al12Si; Additive manufacturing.

1.0 Introduction

Bimetallic structures have attracted much attention recently because of the advantages of manufacturing multi-functional structures in one operation, reducing material weight in a structure, minimizing high temperature joining operations, and related defects. As many products are shifting more towards custom-designed articles, modern manufacturing is also moving from large quantities of the same products to small quantities of highly customized parts that require shape control and properties designed at specific locations. Such structures require know-how related to how to manufacture different materials in a single operation. Traditionally, bimetallic structures are manufactured by joining two different metallic materials via different types of welding. Stainless steel (SS) and Al alloys are the two metallic materials widely used in many industrial applications. SS alloys show excellent corrosion resistance, good strength, and can be used at a broad temperature range. Al alloy has advantages such as a high strength-to-weight ratio, good corrosion resistance, and excellent formability. Exploiting SS to Al bimetallic material could effectively help many applications, including aerospace, shipbuilding, and automobile parts [1,2].

Joining two dissimilar materials together, such as SS and Al12Si alloy, can be very challenging. Since the thermal properties of Al12Si are not available, the thermal properties data of Al 6061-T6 alloy are used here for comparison. **Table 1** shows the thermal properties of SS 316L and Al 6061-T6 [3]. It clearly shows that SS 316L and Al 6061 significantly differ in melting temperature and thermal conductivity, making these two materials very hard to join. Traditionally, welding is the most common technique applied to fabricate SS to Al bimetallic structures. Researchers have joined SS with Al alloy by utilizing different welding techniques such as friction stir welding (FSW), friction crush welding (FCW), metal inert gas (MIG) welding, and cold metal transition [1,4–7]. Some literature reported that SS to Al bimetallic composites were obtained using a compound casting process and hot-dip aluminizing methods

[8,9]. However, there still are some concerns while using these methods to fabricate such bimetallic structures. One of the significant issues in processing bimetallic structures is cracking at the interface due to the brittle intermetallic phase formation. Moreover, using welding techniques to join dissimilar metals could lead to a large heat-affected zone (HAZ). Some other disadvantages include distortion due to residual stresses, and scale formation during joining may limit welding methods, especially FSW, to join steel with Al alloy. These concerns could lead to negative impacts on fabricated bimetallic structures and failure. Therefore, there is a knowledge gap that exists to manufacture Al to SS alloys' bimetallic structures, which is the current work's primary objective.

Table 1. Thermal properties of SS 316L and Al 6061-T6 [3].

Materials	Melting Point (°C)	Coefficient of Thermal Expansion at 250 °C (µm/m°C)	Specific Heat Capacity (J/g°C)	Thermal Conductivity (W/mK)
SS 316L	1370 - 1400	16.2	0.5	16.3
Al 6061-T6	582 - 652	25.2	0.896	167

Additive manufacturing (AM) is a 3D object fabrication technology that converts computer-aided design (CAD) files to real parts layer-by-layer. This technology allows full customization not only in shape but also in the composition of the final products. Metal AM often uses metallic powder or metal wire as feedstock material, and various techniques such as powder-bed fusion (PBF), directed energy deposition (DED), and wire-based additive manufacturing has been developed during the past three decades. Since the fabricated component material can be customized via metal AM technologies, it is possible to fabricate a bimetallic structure additively tailoring the interface compositions instead of joining two metallic materials together. Researchers have demonstrated that metal AM techniques are a feasible way to fabricate various bimetallic structures and studied such structures' properties. Yin et al. showed that an Al-Ti6Al4V bimetallic structure without intermetallic phase formation was fabricated by selective laser melting (SLM) and cold spraying hybrid AM method [10]. Zhang et al. also reported that similar Ti6Al4V to Al12Si bimetallic structures manufactured via the DED method, and a compositionally graded transition section was applied to avoid thermal properties

mismatch [11]. Also, Inconel 718 to Ti6Al4V, Inconel 718 to Cu alloy, Ti6Al4V to SS410, and Ti6Al4V to SS 316 bimetallic structures were reported by the DED technique with good bonding strength [12–15]. Furthermore, researchers reported that the wire arc additive manufacturing (WAAM) method could be utilized to fabricate low-carbon steel (LCS) to SS 316 and steel to bronze thin-wall bimetallic structures [16,17]. Without using a third material as a bonding material, there are two strategies to build a bimetallic structure via metal AM technology: direct bonding and compositionally graded transition. Direct bonding is directly built on one type of metal on top of another. Although most bimetallic structures fabricated by metal AM technology were directly bonded, however, for the bimetallic structures composed of dissimilar materials, the interface could have thermal mismatches at elevated temperatures and fail. Instead of making a "sharp" compositional transition, applying a "smooth" compositionally graded transition zone could avoid the thermal mismatch issue. Researchers have compared the bonding interface of metal AM made Inconel 718 to GRCop-84 bimetallic materials fabricated by utilizing both direct bonding and compositionally graded transition [13]. The results showed that the bimetallic structure, which had compositionally graded transition, had better diffusion at the interface than direct bonding.

To fabricate bimetallic structures with compositionally graded transition via metal AM technology, pre-mixing or *in situ* mixings of powders are needed. Theoretically, a bimetallic structure with compositionally graded transition could be made by using the PBF technique combined with pre-mixed powders. However, this method needs multiple powder changes, which is time-consuming and causes a lot of powder waste due to mixing. The DED is an AM technique that uses metallic powders as feedstock. This method typically utilizes a laser as an energy source and creates a molten metal pool on a substrate when the laser is fired. Then, the metallic powders are fed to the molten metal pool via the carrier gas and liquified. The stage which holds the metal substrate can move in both *X* and *Y* directions to achieve laser scanning. While laser scanning, the previous molten spot experiences rapid solidification. After the first layer is formed, the laser head moves up in the *Z* direction and repeats the laser scanning procedure until the 3D object is formed. The working chamber is sealed with a glove box and filled with inert gas to prevent oxidation during processing. Multiple powder feeders could be installed on a DED system, and each powder feeder can be controlled individually. This feature allows *in situ* powder mixing without pausing the fabrication processing, which could be an

efficient method of dynamically making a compositionally graded transition to bond two metallic materials. Processing parameters such as laser power, laser scan speed, and powder feed rate can also be adjusted during the processing based on the part geometry and composition. In this study, the compositionally graded interface was created to fabricate SS 316L to Al12Si bimetallic structures with a commercial DED-based AM system. This research aimed to study the influence of processing parameters on microstructure, phase formation, microhardness, and compressive deformation of the fabricated bimetallic structures.

2.0 Materials and methods

2.1 Laser processing of SS 316L to Al12Si bimetallic structures with compositional gradation: Spherical SS 316L powder (ASTM F2792M, 17% Cr, 12% Ni, 2.5% Mo, 1.5% Mn, 0.85 Si and 0.02% C, Höganäs, Belgium) with a powder particle size range of 53 μm to 150 μm, and spherical Al12Si powder (Grade S20, Valimet Inc., Stockton, CA) with a powder particle size range of 48 μm to 105 μm were used. Additional powder sieving was applied to achieve the best print results. A mechanical sieve shaker was utilized, and each type of powder was sieved for 15 min. Only the powders with particle size range from 45 μm to 150 μm (-100/+325 mesh) were collected. A SS 316 plate (Tiger Metals Group, Los Angeles, CA) with a thickness of 3.5 mm was selected as a metal substrate. A DED system (FormAlloy, Spring Valley, CA) with two powder feeders was employed to fabricate SS 316L to Al12Si bimetallic structures. Each powder feeder was loaded with one type of metallic powder. The DED system uses optical fiber as the laser source and can achieve 500 W laser power, and the working chamber was purged with argon gas to reduce the oxygen level below 20 ppm. A cooling system was installed and kept the working stage temperature at 15 ℃ during processing. Both square and cylindrical SS 316L to Al12Si bimetallic structures were designed. **Fig. 1a** demonstrates the design of the DED made SS 316L to Al12Si bimetallic structure. Each bimetallic structure was composed of three sections: a pure SS 316L section, a compositionally graded transition section, and a pure Al12Si section. The designed square shape structure had a dimension of 20 mm x 20 mm (length x width), and the cylindrical structure had a diameter of 10 mm. Also, the in-fill scan orientation was configured as 0 and 90 degrees (**Fig.1b**), the hatch distance was set to 0.417 mm, and the in-fill scan speed was set to 1200 mm/min. A schematic of the DED processing is illustrated in **Fig.**

1c. Multiple manufacturing attempts were performed to optimize the processing parameters. **Table 2** shows details of the processing parameters of the bimetallic structures fabricated via DED. Two approaches were tried using different processing parameters to understand the effects caused by the processing parameters and composition. Specifically, 30 layers of pure SS 316L section was first deposited for both approaches using a laser power of 250 W and a layer thickness of 0.15 mm. Only powder feeder 1 (SS 316L) was opened to fabricate the pure SS 316L section with a 21.5 g/min powder feed rate. A SS 316L to Al12Si compositionally graded transition was built after the pure SS 316L section. Both powder feeder 1 and 2 were used during this part of manufacturing.

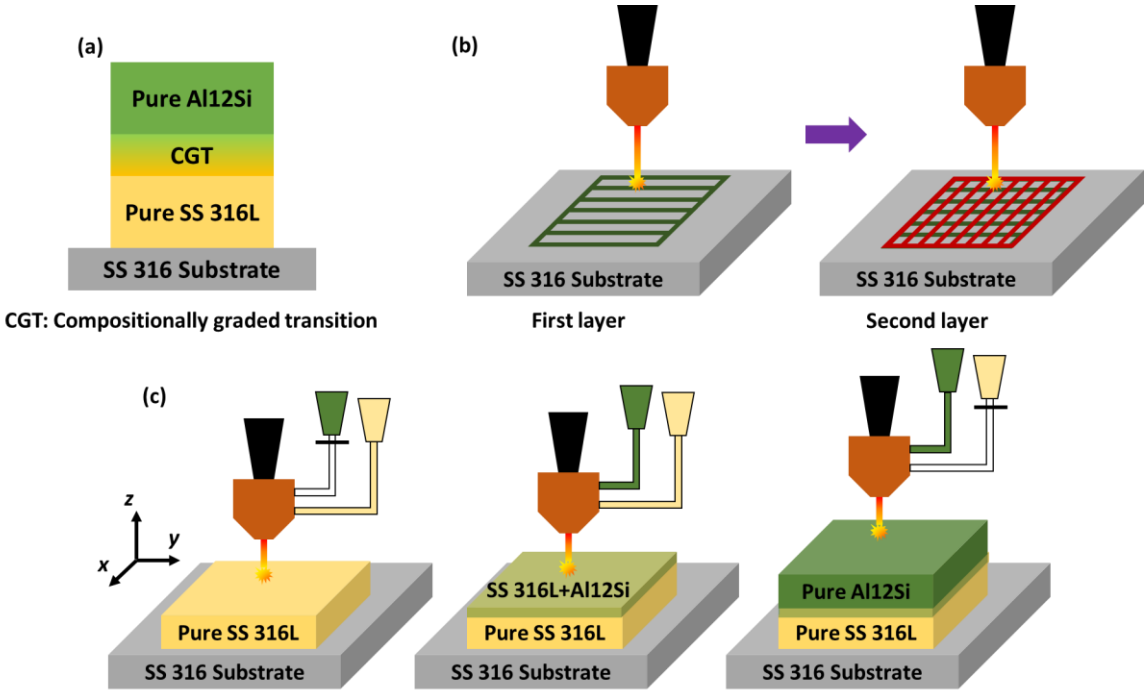

Figure 1. (a) Design of the DED fabricated SS 316L to Al12Si bimetallic structure. (b) Schematic of the orientation of the laser scanning path (0°, 90°). (c) Schematic of the manufacturing processing of SS316L to Al12Si bimetallic structure via DED.

Table 2. Processing parameters of DED fabricated SS 316L to Al12Si bimetallic structures.

Sample	*Section*	*Layer Number*	*Laser Power (W)*	*Powder Feed Rate (g/min)*		*Hatch Scan Speed (mm/min)*	*Layer Thickness (mm)*
				Powder Feeder 1 (SS 316L)	*Powder Feeder 2 (Al12Si)*		
Approach 1	Pure SS 316L	1-30	250	21.5	0	1200	0.15
	$(SS\ 316L+Al12Si)_1$	31-40	240	18.4	1.3	1200	0.16
	$(SS\ 316L+Al12Si)_2$	41-50	230	3.1	8.4	1200	0.20
	Pure Al12Si	51-60	200	0	9.5	1200	0.25
Approach 2	Pure SS 316L	1-30	250	21.5	0	1200	0.15
	SS 316L+Al12Si	31-34	230	3	8.4	1200	0.20
	Pure Al12Si	35-55	200	0	9.5	1200	0.25

Different strategies were used to build this transition section. For approach 1, the compositionally graded transition consisted of two parts: $(SS\ 316L+Al12Si)_1$ and $(SS\ 316L+Al12Si)_2$. Each of these sections had 10 layers, and the layer thicknesses were 0.16 mm and 0.20 mm, respectively. Laser power was adjusted to 240 W to fabricate $(SS\ 316L+Al12Si)_1$ section. The powder feed rates of SS 316L and Al12Si in this section were set as 18.4 g/min and 1.3 g/min, respectively. $(SS\ 316L+Al12Si)_2$ was fabricated using a laser power of 230 W with 3.1 g/min of the powder feed rate of SS 316L and 8.4 g/min of the powder feed rate of Al12Si. For approach 2, the transition section was made by a single mixed composition, and the processing parameters were similar to approach 1's $(SS\ 316L+Al12Si)_2$, but only had 4 layers. Both approaches used the same processing parameters to fabricate the pure Al12Si section. The pure Al12Si section had 20 layers in total, and the laser power was reduced to 200 W to fabricate this section while the layer thickness was increased to 0.25 mm. Only powder feeder 2 (Al12Si) was opened, and the powder feed rate of Al12Si was 9.5 g/min.

2.2 Characterization: A low-speed diamond saw (MTI, Richmond, CA) was utilized to cut the as-fabricated samples for exposing the cross-section. Surface finishing was then applied to the exposed cross-sections. The sectioned samples were ground by sandpapers with grits from

200 to 2000, then polished with Al_2O_3 suspension with particle size from 1 μm to 0.05 μm. Samples were immersed in a 50% ethanol solution and cleaned by an ultrasonicator for 20 mins.

Heat-treatment, microstructure, and phase analyses: Samples fabricated using approach 2 were heat-treated (HT) at 300°C for 1h and then furnace cooled to room temperature. The heat-treated samples were sectioned to examine the microstructure at the cross-section. Two types of etching reagents were utilized. Keller's reagent (95 mL of DI water, 2.5 mL of HNO_3, 1.5 mL of HCl, and 1 mL of HF) was used to reveal the microstructure of Al12Si, and Carpenter 300 series etchant (8.5 g of $FeCl_3$, 2.4 g of $CuCl_2$, 122 mL of ethanol, 122 mL of HCl, 6 mL of HNO_3) and was utilized to etch SS 316L composition. Cotton swabs were used to help apply each etching reagent to the target sections. The pure Al12Si section and SS 316L+Al12Si section were etched with Keller's reagent for 30 seconds, and the pure SS 316L section was swabbed with Carpenter etchant for 40 seconds. The microstructures at the cross-section of fabricated bimetallic samples were obtained by both Scanning Electron Microscope (SEM) and optical microscope. X-ray diffraction (XRD) analysis was performed on the cross-section of the DED fabricated SS 316L to Al12Si bimetallic structures using a Siemens D 500 Kristalloflex diffractometer. Cu-K_α was selected as a radiation source, a 2θ from 20 to 80 degrees, and 0.05-degree step size were applied for analysis. Also, the elemental distribution at samples' cross-section was analyzed using energy-dispersive X-ray spectroscopy (EDS).

Microhardness and compression tests: The microhardness data at the cross-section was obtained from a microhardness tester (Phase II, NJ). The hardness test used a testing load of 0.9807 N ($HV_{0.1}$) and a dwell time of 15s. Multiple indentations were applied across the interface and at the same depth. The hardness value at each depth was averaged based on measurements. The cylindrical specimens were prepared from the samples manufactured using approach 2 with a CNC machine. The cylindrical specimens were machined with an initial length (L_0) to diameter (D) ratio of $L_0/D \approx 1.5$. A SHIMADZU AG-1S (50 KN) screw-driven universal testing machine was used for compression tests. The compression tests were performed by following ASTM E9-09 [34]. Both HT and non-HT specimens were tested.

3.0 Results

Fig. 2 demonstrates the images of as-fabricated bimetallic structures and their cross-sections processed by both approaches. Based on the results of the first approach (**Fig. 2a**), each section can be clearly distinguished on the square shape bimetallic structure. Also, visible cracks could be seen at the interface between the pure SS 316L section and the $(SS\ 316L+Al12Si)_1$ section. After the sample was sectioned (**Fig. 2b**), the location where the cracks were found showed a gap to highlight the extent of deformation due to thermal mismatch. However, no cracks were observed at the interface between the $(SS\ 316L+Al12Si)_2$ section and the pure Al12Si section. Based on this knowledge, during the second approach, the $(SS\ 316L+Al12Si)_1$ from the previous design was removed, and the transition section had only 4 layers. **Fig. 2c** demonstrates the as-fabricated square shape SS 316L+Al12Si bimetallic structure with optimized design, and **Fig. 2d** shows the cylindrical bimetallic structure fabricated using the same design as **Fig. 2c** after surface machining. In **Fig. 2c**, no visible cracks or delamination were found at the interface between the pure SS 316L and the pure Al12Si sections. Although the cylindrical bimetallic structure showed in **Fig. 2d** had some pores at the interface region, but these defects only remained at the surface and did not penetrate inside of the sample.

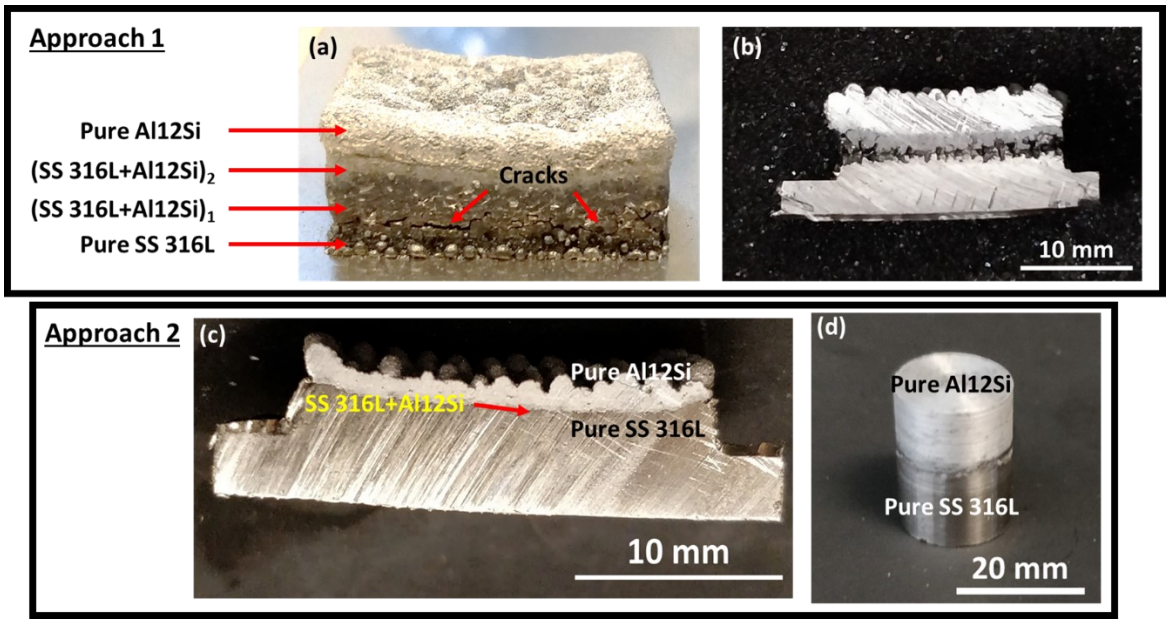

Figure 2. (a) As-fabricated SS 316L to Al12Si bimetallic square-shape samples fabricated by approach 1. Visible cracks were observed. (b) The cross-section surface of approach 1. Poor bonding between pure SS 316L section and $(SS\ 316L+Al12Si)_1$ can be seen. (c) The cross-section of as-fabricated from approach 2. (d) Cylindrical SS 316L to Al12Si bimetallic structure after surface machining.

The microstructure of SS 316L to Al12Si bimetallic structures: Most of the characterization was done on the samples made from approach 2 since approach 1 samples had extensive cracks at the interface. Microstructures of each section of the DED processed SS 316L+Al12Si bimetallic structures were studied and shown in **Fig. 3**. Specifically, **Fig. 3a** reveals microstructure at the interface between the SS 316 substrate and the DED made pure SS 316L section. The SS 316 substrate was dominated by coarse equiaxed grains, while the acicular microstructures were found in the deposited SS 316L section. Additionally, the acicular microstructures found in the pure SS 316L section had a specific orientation. No pores and cracks were found at this interface. **Fig. 3b** illustrates microstructures at the pure SS 316L section. Both acicular microstructures and fine equiaxed grains can be seen. The acicular microstructures were mainly found at the first few layers, and the fine equiaxed grains were formed at the layers that were built away from the substrate. Moreover, the acicular microstructures had an orientation towards the building direction. **Fig. 3c** shows the microstructures at the compositionally graded transition. Micro-cracks and unmelted particles can be seen at this location. Micro-cracks were not connected, and each crack propagated horizontally along with the layer. Furthermore, a reaction zone was found near the interface and towards the pure Al12Si region. Fine dendritic microstructures were found in the reaction zone. **Fig. 3d** demonstrates the morphology at the compositionally graded interface after heat treatment. Compared to **Fig. 3c**, the intermetallic phases were partially diffused after heat treatment. **Fig. 3e** illustrates the microstructures at the pure Al12Si section. The Si particles were embedded in the Al matrix.

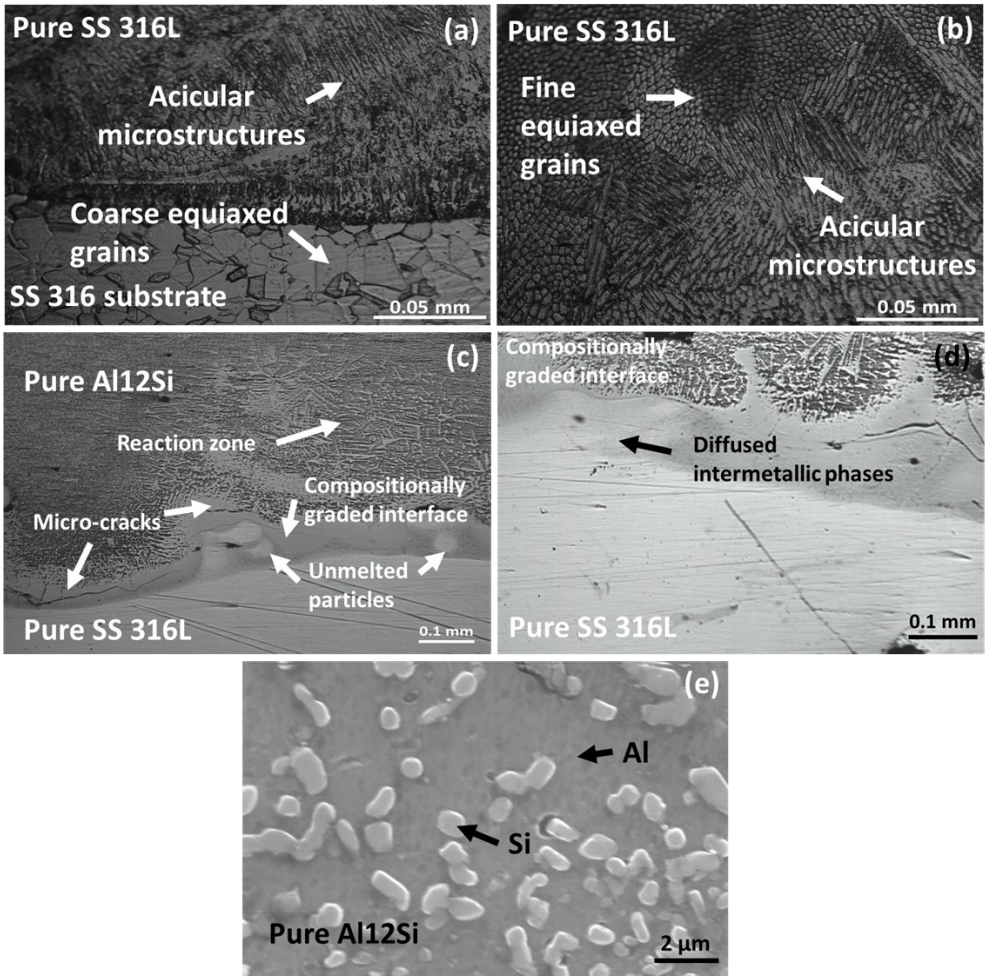

Figure 3. The microstructures at the sample's cross-section from approach 2. (a) The microstructures at the SS 316 substrate interface and pure SS 316L. (b) The microstructures at the pure SS 316L section. (c) The microstructures at compositionally graded transition region. (d) The microstructures at compositionally graded transition region after heat treatment. (e) The microstructures at pure Al12Si region.

Elemental distribution, phase analysis, microhardness test, and compression test: The elemental distribution analysis was performed at the compositionally graded transition section. **Fig. 4** shows the EDS mapping of the selected elements. Based on the results, the concentration of Fe and Cr were gradually decreased from bottom to top while the concentration of Al and Si were gradually increased. The EDS results also show the unmelted particle was a SS 316L particle, and the dendritic structures contained both Fe and Al elements. **Fig. 5a** shows the XRD results at the compositionally graded transition of SS 316L to Al12Si bimetallic structures.

According to the XRD profile, new phases such as FeAl, Fe_2Al_5, and $FeAl_3$ were formed during laser processing.

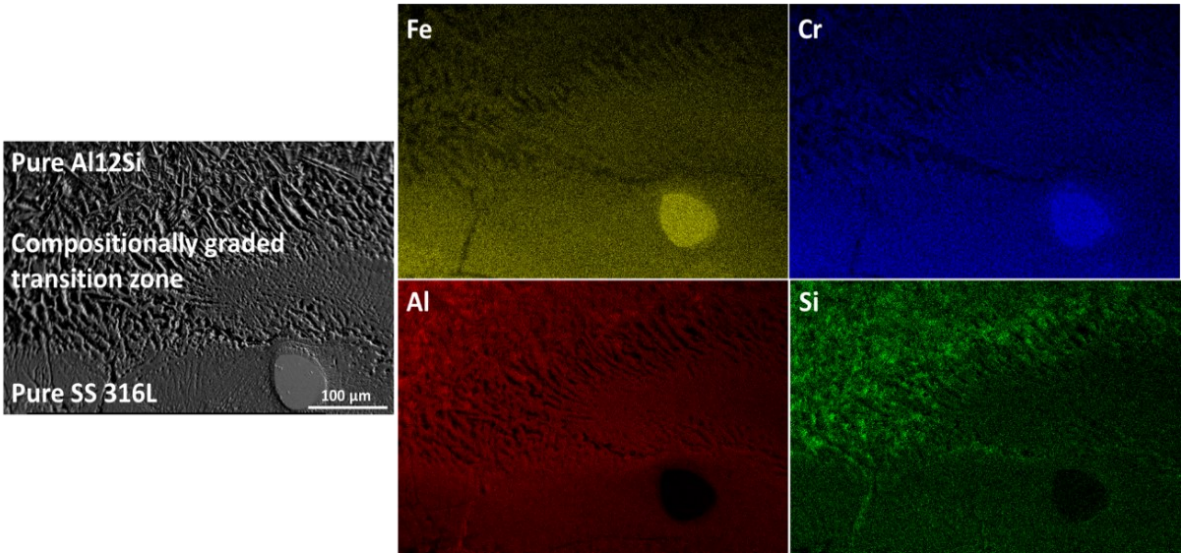

Figure 4. EDS mapping at the compositionally graded transition zone of the sample from approach 2.

Fig. 5b is the microhardness results of the samples which were fabricated using approach 2. Additionally, the microhardness tests were performed on both non-HT and HT samples. The hardness of each section was measured. According to the non-HT sample measurements, the SS 316 substrate's hardness was 197.1 ± 2.1 $HV_{0.1}$. The hardness increased to 237.8 ± 9.2 $HV_{0.1}$ in the DED made pure SS 316L section. Also, the microhardness in the pure SS 316L section increased near the compositionally graded transition area. The hardness of the compositionally graded transition area had the highest hardness among the entire cross-section, 834.2 ± 107.1 $HV_{0.1}$. Hardness values were only measured at two different depths in this section due to the thin layers. Furthermore, the DED made pure Al12Si section had the lowest hardness of 63.2 ± 6.2 $HV_{0.1}$. The microhardness values of the HT sample at SS 316 substrate, pure SS 316L, and pure Al12Si sections were 203.6 ± 20.5 $HV_{0.1}$, 239.3 ± 15.9 $HV_{0.1,}$ and 76.5 ± 4.4 $HV_{0.1}$, which were similar to the hardness values of the non-HT sample at the same regions. However, the HT sample's hardness at the compositionally graded transition section was 578.7 ± 154.1 $HV_{0.1}$, which was ~30% lower than the hardness of the non-HT sample. Based on the results of compression tests (**Table 3**), the maximum compressive stresses of both non-HT and HT DED

processed SS 316L/Al12Si bimetallic were 299.4 ± 22.1MPa and 270.1 ± 27.1 MPa, respectively.

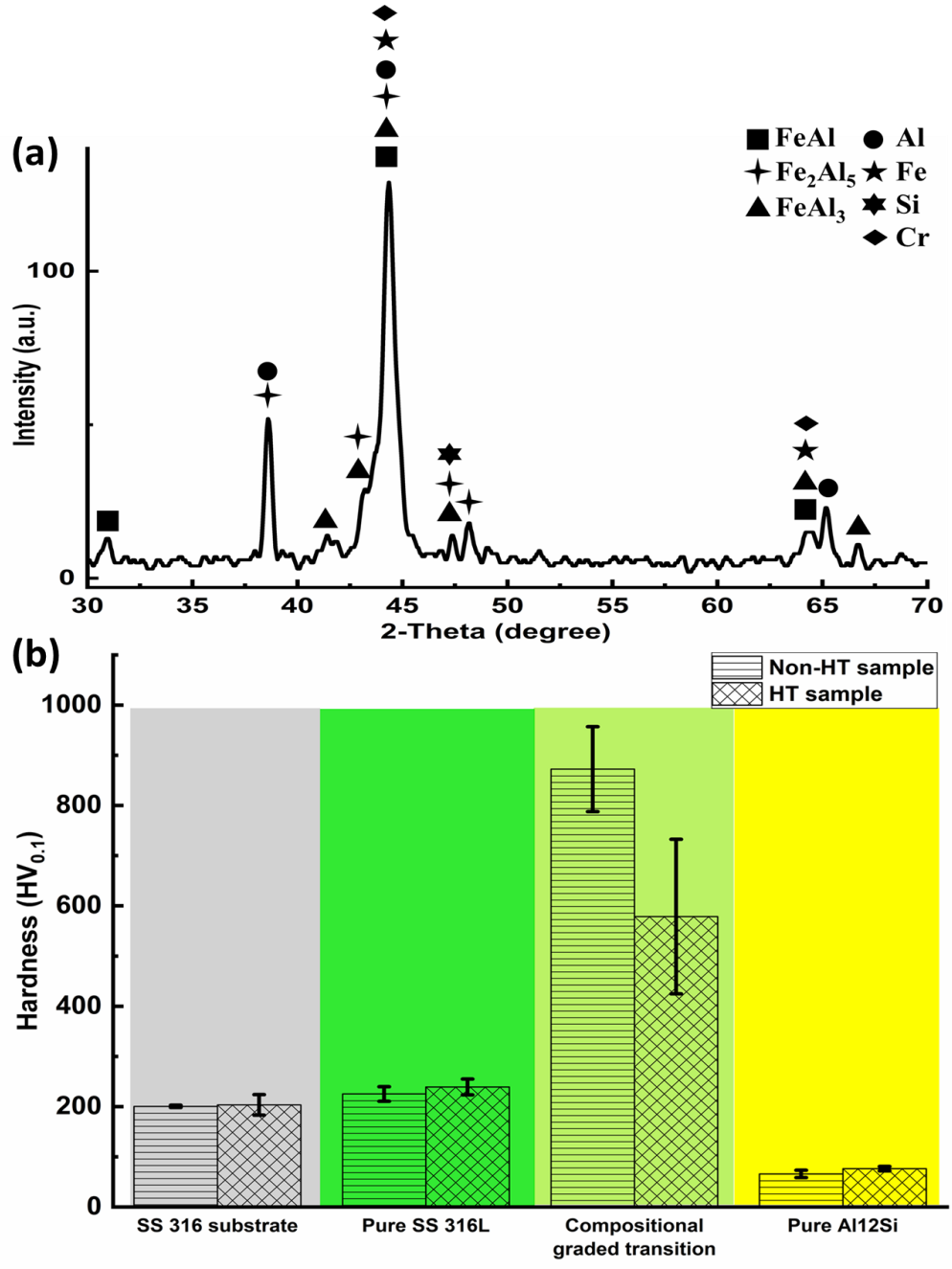

Figure 5. (a) XRD data at the compositionally graded transition zone of the sample from approach 2. (b1) Hardness profile at the cross-section of both the HT and the non-HT samples from approach 2. (b2) Schematic of microhardness tests performed on the cross-section of specimen.

Table 3. Comparison of maximum compressive stress of bimetallic structures with different Al alloys.

Material	Maximum Compressive Stress (MPa)
DED processed **SS316L/Al12Si** bimetallic material **(non-HT**)	**299.4 ± 22.1**
DED processed **SS316L/Al12Si** bimetallic material **(HT**)	**270.1 ± 27.1**
Al AA6082 T6 [35]	**290**
Al AA2024 T4 [36]	**476**
Al AA6111 [37]	**272**

Fig. 6a and 6b illustrate the images of SS 316L/Al12Si cylindrical specimens before and after the compression tests. Pure Al12Si sections were the primarily deformed region for both non-HT and HT specimens. Additionally, vertical cracks can be seen from the pure Al12Si section of both specimens after compression tests. These vertical cracks did not penetrate the pure SS 316L section. **Fig. 6c and 6d** are the optical microphotographs at the interface between pure SS 316L and compositionally graded transitions of both non-HT and HT SS 316l/Al12Si cylindrical specimens after the compression tests. Cleavage patterns were obtained in the compositionally graded transition area for both non-HT, and HT fractured specimens. Additionally, discontinued cracks and pores were also found along with the interface between pure SS 316L and compositionally graded transition of both samples.

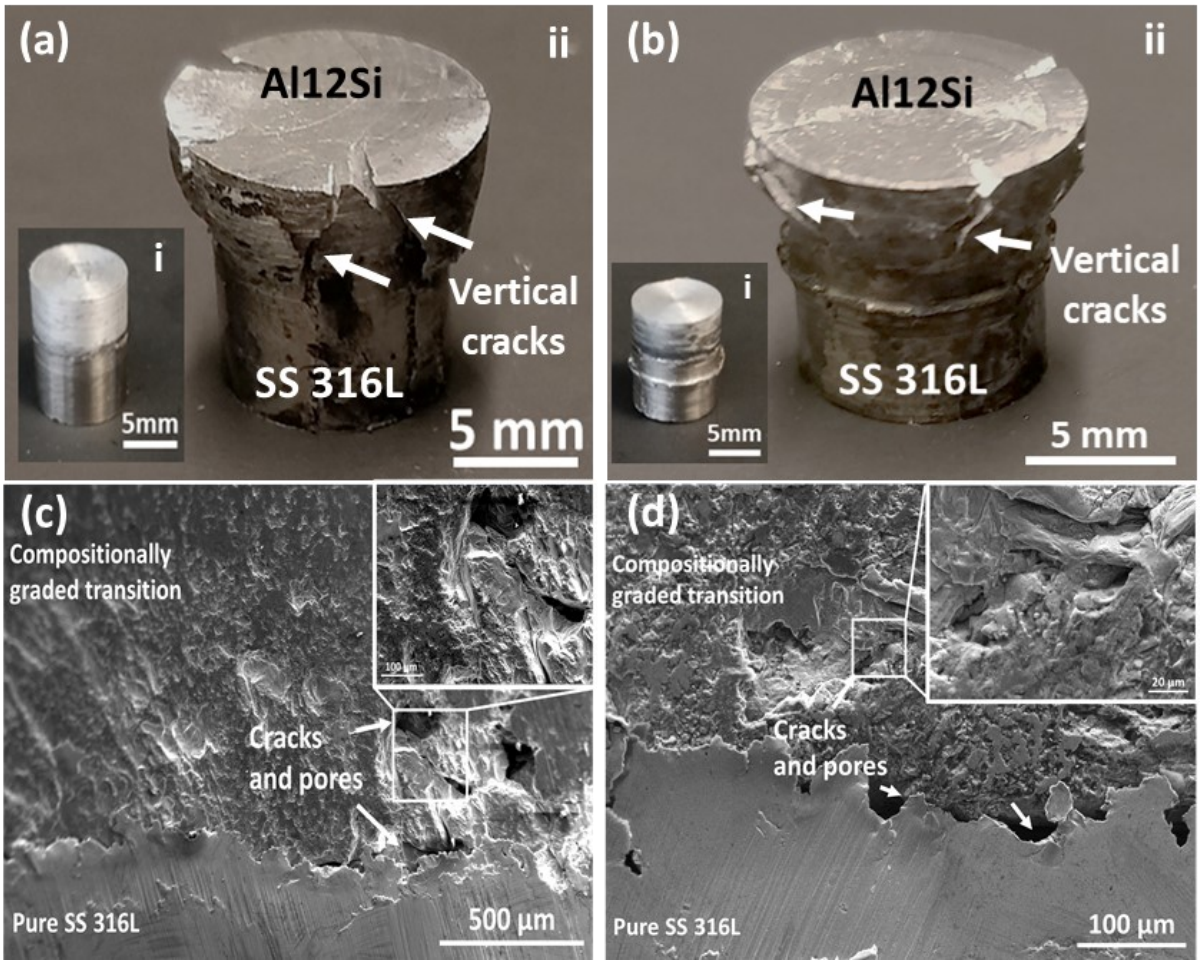

Figure 6. (a) Images of non-HT SS 316L/Al12Si cylindrical specimen, (i) before the compression test, (ii) after the compression test. (b) Images of HT SS 316L/Al12Si cylindrical specimen, (i) before the compression test, (ii) after the compression test. (c) After the compression test, the fracture surface of the non-HT SS 316L/Al12Si cylindrical specimen at the interface between pure SS 316L and compositionally graded transition occurs. (d) After the compression test, the fracture surface of the HT SS 316L/Al12Si cylindrical specimen at the interface between pure SS 316L and compositionally graded transition occurs.

4.0 Discussion

One of this work's objectives was to explore the feasibility of fabricating SS 316L to Al12Si bimetallic structures via DED technology. The multiple powder feeders and the real-time control over each powder feeder features of a DED system allow *in situ* powder mixing during

processing. By taking these advantages, bimetallic structures processed by DED show a "smooth" compositionally graded transition zone with minimal defects. Compared to bimetallic structures that directly bond two metallic materials, the bimetallic structures that have a compositionally graded transition could reduce the two metals' property mismatches. This feature could be significant, especially for bonding two dissimilar metallic materials. Also, the fabrication of a bimetallic structure without introducing a third bonding material is more comfortable to control properties if such structures can be processed. Although brittle intermetallic phases formed in the compositionally graded transition of a DED processed bimetallic material, the intermetallic phase formation could be minimized by reducing the number of transition layers and processing parameter optimization. And that was the main difference between approach 1 and approach 2 for this study. Processing parameters optimization is the most critical factor to fabricate a bimetallic material successfully via DED. Processing parameter optimization includes the parameter adjustment of pure materials and the compositionally graded transition. Several trials were conducted to optimize the processing parameters of each section (**Fig. 7**). Previous studies have demonstrated using the DED method to fabricate pure SS [18–21] and Al alloys [22–24]. However, the processing parameters vary based on each DED system. The specific energy input equation was utilized [25] to determine the suitable processing parameters for this study's design.

$$E = \frac{P}{v \times h \times t}$$

where E is specific energy input, P is laser power, v is laser scan speed, h is hatch distance, and t is layer thickness. First, the specific energy inputs for the DED processed pure SS 316L and Al alloys were calculated based on the literature data. Then, using that E value, laser power, and layer thicknesses were predicted for our design. Specifically, the bimetallic structure's design had a hatch distance of 0.417 mm, and a constant laser scan speed of 1200 mm/s. Additionally, based on several trials' results, the minimum laser power required to melt SS 316L and Al12Si powder was established. Hence, the layer thickness of each pure metal section could be estimated. **Fig. S1** and **S2** show the optimization process for the DED processed pure SS 316L and pure Al12Si. According to the testing runs, the processing parameter of the pure SS 316L and pure Al12Si were determined and shown in **Table 2**. The optimized laser power and powder feed rate for fabricating SS 316L and Al12Si were 250 W and 200 W, 21.5 g/min and 9.5 g/min, respectively.

The processing parameter optimization progression at the compositionally graded transition section of the DED fabricated SS 316L to Al12Si bimetallic structure is summarized in **Table 4**. The listed samples in **Table 4** correlates to the samples demonstrated in **Fig. 7**. Specifically, samples 1 to 4 were processed for laser power optimization at the compositionally graded transition section. According to the results, sample 1 showed critical delamination at the interphase between the Al-rich SS 316L+Al12Si section and the pure Al12Si section. This phenomenon was caused by high laser power that was introduced in the delaminated region. Reduced laser power was 230 W helped to eliminate the delamination problem in Sample 3. However, visible cracks could still be seen at the interface between the pure SS 316L section and SS 316L-rich SS 316L/Al12Si section, even though the laser power was reduced to 240 W (Sample 4). Such cracking behavior could be caused due to thermal properties mismatch between the two sections. Sample 5 to 8 were for optimizing powder feed rates for both SS 316L and Al12Si at the transition section. To avoid thermal properties mismatch, reducing decrements/increments of SS 316L/Al12Si powder feed rates were tried to obtain a full compositional gradient. The results showed that sample 8 had minimum cracks based on only visual observation. Moreover, **Fig. 2, S3,** and **S4** were the progression of further parameter optimization at the compositionally graded transition. The design of the SS 316L/Al12Si bimetallic structure from approach 1 had a $(SS\ 316L+Al12Si)_1$ section and a $(SS\ 316L+Al12Si)_2$ section, which were SS 316L dominated and Al12Si dominated, respectively. The sample's cross-section image from approach 1 (**Fig. 2b**) showed a gap at the interface between the pure SS 316L and $(SS\ 316L+Al12Si)_1$, which indicates poor bonding between these two sections. Poor bonding caused visible cracks along with the interface of these two sections (**Fig. 2a**). A possible explanation of the gap formation is that many brittle intermetallic phases formed near this area during the DED operation. The brittle intermetallic phases had poor thermal shock resistance and cracked due to rapid solidification. However, no such cracking or gap formation occurred at the interface between $(SS\ 316L+Al12Si)_2$ and pure Al12Si section, indicating good diffusion of these two compositions and fewer amounts of brittle intermetallic phase formation. A new bimetallic structure was designed with a compositionally graded transition that used one mixed composition to overcome the poor bonding issue at the interface. **Fig. S3** shows the DED processed SS 316L/Al12Si bimetallic structures with a SS 316L dominated SS 316L+Al12Si transition section only. Each sample was fabricated with a different number of transition layers.

According to the results, only the sample with 4 layers of SS 316L dominated SS 316L+Al12Si mixed composition had no visible defects. However, the optical microscope image at the interface still showed a micro-gap between the SS 316L+Al12Si and pure Al12Si. **Fig. S4** shows the DED processed SS 316L/Al12Si bimetallic structures with an Al12Si dominated SS 316L+Al12Si transition section only. The effect of the number of transition layers on bonding performance was also studied. Based on the results, no visible defects could be seen on all as-fabricated bimetallic structures. The microscope analysis of samples' cross-section showed that the sample with 4 transition layers had the best bonding performance, which had no micro-gap between each section, and the micro-cracks were minimized. With this knowledge, the bimetallic structure design for approach 2 only used one mixed composition, which was similar to the (SS 316L+Al12Si)$_2$ section from approach 1. The number of graded transition layers was reduced to 4 layers instead of 10 layers to minimize the brittle intermetallic phase formation during the DED processing. Based on the results of **Fig. 2c**, the cross-section of the as-fabricated samples from approach 2 showed a significant improvement at the interface between the pure SS 316L and pure Al12Si compared to the previous approach. No visible defects could be seen at the interface. **Fig. 2d** demonstrated the cylindrical shape SS 316L to Al12Si bimetallic structure after surface machining. A CNC lathe machine was utilized for the surface finishing, which means the DED fabricated SS 316L to Al12Si bimetallic structure could be processed by conventional machining for any application.

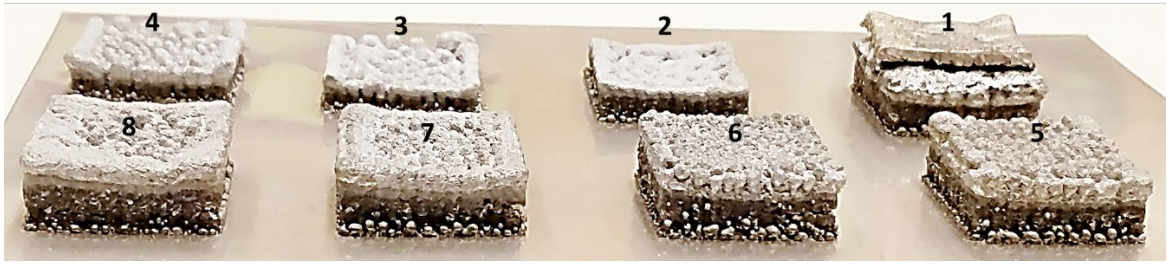

Figure 7. DED-based processing parameter optimization for SS 316L to Al12Si bimetallic structures.

Table 4. Processing parameter optimizations for the compositionally graded transition of DED fabricated SS 316L to Al12Si bimetallic structures.

Sample	Laser power for SS 316L-rich sections (W)	Laser power for Al12Si-rich sections (W)	Decrements of SS 316L powder feed rate per layer (g/min)	Increments of Al12Si powder feed rate per layer (g/min)
1	250	250	1	1
2	250	240	1	1
3	250	230	1	1
4	240	230	1	1
5	240	230	0.9	0.9
6	240	230	0.8	0.8
7	240	230	0.7	0.7
8	240	230	0.6	0.6

Fig. 3 reveals microstructural variations in each section of the DED fabricated SS 316L to Al12Si bimetallic structure. Compositional variations mainly cause microstructural variations. **Fig. 3a** shows the interface between the SS 316 substrate and the DED processed pure SS 316L. Although these two sections' composition is the same, the difference in microstructure was caused due to processing. The as-received SS 316 substrate had coarse equiaxed grains, which are typically a signature from annealing. The DED processed SS 316L had both acicular and fine equiaxed microstructures (**Fig. 3a and Fig. 3b**). The acicular microstructures were mainly found at the bottom layers, near the substrate, and the fine equiaxed microstructures were generally obtained at the top layers. These microstructural variations were caused due to the cooling rate differences during the DED processing. The DED system used in this study has a stage temperature controller, which keeps the metal substrate's temperature at 15 °C during the laser processing. Therefore, the initial layers experienced a higher cooling rate compared to the layers deposited later. This high cooling rate leads to complex and non-equilibrium solidification conditions, which limited the time for grains to grow. Also, the high cooling rate prevents the acicular microstructure from developing secondary dendritic arms. Moreover, the formed acicular microstructures grew towards the heat flow direction. Zheng et al. also showed that the convective flow during the DED processing could dissipate the superheat in the molten metal pool to provide suitable grain growth location and orientation for the acicular microstructures [26]. A lower cooling rate caused the formation of fine equiaxed grains at the pure SS 316L section. As the laser processing continued, the residual heat from the previous layers could

reduce the cooling rate. However, this cooling rate is still greater than the conventional heat treatments such as annealing or normalizing. The fine equiaxed grains are primary γ-austenite cells with intercellular δ-ferrite. The phase transformation of SS 316L during solidification can be shown as L → (γ+L) → (γ+δ+L) → (γ+δ) → γ [27]. The lower cooling rate allows sufficient time to form γ+δ during solidification. The formations of both acicular and equiaxed microstructures of the DED fabricated SS 316L were also reported in previous studies [26–30]. **Fig. 3c** demonstrates the microstructures at the compositionally graded transition area. Discontinued micro-cracks and unmelted particles can be seen in this region, suggesting that further processing parameters optimization is needed. Based on the EDS results (**Fig. 4**), the Fe and Cr distribution concentration decreased from the bottom to the top, while the Al and the Si concentrations increased. The results of EDS mapping are the evidence to confirm the compositional gradation at the interface region. The EDS results also confirmed that the unmelted particles were SS 316L. A reaction zone with dendritic microstructures can be seen near the interface but towards the pure Al12Si section. The XRD results (**Fig. 5a**) showed that FeAl, Fe_2Al_5, and $FeAl_3$ intermetallic phases are formed at this location. From **Table 2** approach 2, the applied processing parameters for fabricating the compositionally graded transition used an Al12Si dominated composition. Also, *in situ* mixing technique was utilized to fabricate the compositionally graded transition section. This study's DED system can gradually change the powder feed rate for each powder feeder until it reaches the set value. In this case, the target powder feed rates of SS 316L and Al12Si were 3 g/min and 8.4 g/min, respectively. Based on each powder's composition and the powder feed rates, the weight percentage of Fe and Al at the final mixed composition could be calculated, which are 21.2 wt% and 78.8 wt%, respectively. Therefore, Fe and Al's weight percentage in the compositionally graded transition section varied from 100 wt% of Fe and 0 wt% of Al to 21.2 wt% of Fe and 78.8 wt% of Al. The Fe-Al binary phase diagram (**Fig. 8**) shows the conditions of Fe_xAl_y intermetallic phase formation. Researchers have reported that the FeAl could be formed during solidification if the temperature is above 1200 ℃ [1]. Although only a few unmelted SS 316L particles are present at the compositionally graded transition section, the generated temperature was still high enough to create conditions to form the FeAl phase. The required temperatures for forming $FeAl_2$, Fe_2Al_5, and $FeAl_3$ during solidification are 1165 ℃, 1159 ℃, and 1160 ℃, respectively. Theoretically, these phases could be formed during laser processing since those conditions were satisfied.

However, the formation of the $FeAl_2$ phase requires a narrow Fe/Al weight ratio, which is hard to obtain during processing. No Fe_xSi_y, Al_xSi_y, and Cr_xSi_y phases were observed from XRD results. The possible explanation could be either these silicide phases are amorphous, or only a small quantity of silicide phases was formed, which could not be detected. Yuan et al. studied the solubility of Si in Fe alloys, and the results had shown that the solubility of Si in Fe alloy was 6.5 wt% when the temperature was above 1200 ℃ [31]. Such results could validate our finding to show that the silicide phases could hardly be formed during the DED processing. **Fig. 3d** demonstrates the morphology at the HT SS 316L/Al12Si sample compositionally graded transition area. Based on a previous study, Fe atoms require lower activation energy to react with the Fe_xAl_y intermetallic phases compared to Al atoms. Therefore, during the heat treatment, the Fe atoms could interact with existed Al dominated Fe_xAl_y intermetallic phases ($FeAl_3$ and Fe_2Al_5) to form more Fe dominated Fe_xAl_y intermetallic phases (FeAl and Fe_3Al) [38].

Fig. 5b shows the microhardness variation in each section. For both non-HT and HT samples. The results showed that the DED fabricated pure SS 316L section had a higher hardness value compared to the SS 316L substrate. The increase of hardness was due to the microstructural refinement and residual stress. The residual stress caused by laser processing contributes to the higher hardness. For non-HT samples, the microhardness at the compositionally graded transition section was 834.2 ± 107.1 $HV_{0.1}$. This high hardness value was caused due to formations of Fe-Al intermetallic phases. **Table 5** shows the microhardness values of different Fe-Al intermetallic compounds. The microhardness value obtained at the compositionally graded transition section agreed with the hardness value of $FeAl_3$. This hardness value also proved that the $FeAl_3$ phase was dominated at the interface. For the HT sample, the microhardness at the compositionally graded transition section was reduced to 578.7 ± 154.1 $HV_{0.1}$ compared to the non-HT sample in the same region. Fe caused this reduction of hardness dominated Fe_xAl_y intermetallic phases formed during the heat treatment. FeAl phase was more likely to be partially formed during the heat treatment based on this hardness value. This hardness value also proves that heat treatment could reduce the brittleness at the DED's compositionally graded transition made SS316L/Al12Si bimetallic material.

Based on the compression testing results, **Fig 6a** and **6b**, pure Al12Si section was primarily deformed in both non-HT and HT SS 316L/Al12Si bimetallic specimens. Vertical

cracks were found near the edge of both specimens' pure Al12Si section due to high-stress concentration near the ductile material's edge during the compression test. Researchers have demonstrated a finite element (FE) model of an AA6082-T6 cylindrical specimen while experiencing room temperature compression tests. The numeral model also showed higher stress concentration at the specimen's edge during the compression test [39]. **Fig. 6c** and **6d** illustrate the fractography at the interface between the SS 316L and compositionally graded transition of non-HT and HT specimens, respectively. Cleavage, a typical phenomenon obtained from brittle failure, was mainly found in the compositionally graded transition area. The cleavage fractography also proved the brittle intermetallic phase formation in the compositionally graded transition. Additionally, cracks and pores were also found at the interface of both non-HT and HT specimens. The cracks' gap width expanded after the compression test compared to the specimen without experiencing compression test (**Fig. 3c** and **3d**). The expansion of cracks' width was caused by detachment of broken, brittle intermetallic pieces during the compression test. Furthermore, pores' formation was caused by the detachment of unmelted particles from the brittle intermetallic matrix during the compression test. According to **Table 3**, the maximum compressive strength of non-HT and HT SS 316L/Al12Si bimetallic were similar. Table 3 also reports the maximum compressive stress of other Al alloys.

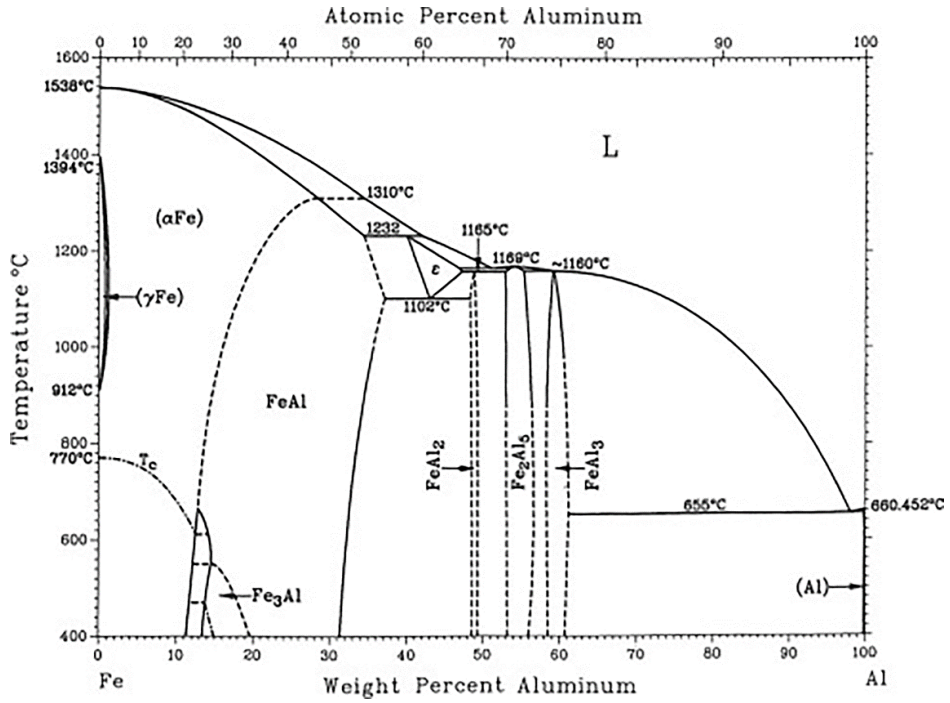

Figure 8. Fe-Al binary phase diagram [32].

Table 5. Microhardness values of Fe-Al intermetallic compounds [33].

Phase	Al content (atomic percentage)	Microhardness (HV)
Fe_3Al	25	250-350
FeAl	50	400-520
Fe_2Al_7	63	650-680
$FeAl_2$	66-67	1000-1050
Fe_2Al_5	69.7-73.2	1000-1100
$FeAl_3$	74-76	820-980

5.0 Conclusions

This study's objective was to fabricate SS 316L to Al12Si bimetallic structures with a compositionally graded transition via the DED technology. The fabricated SS 316L to Al12Si bimetallic structures from two different approaches showed that processing parameters significantly impacted the DED processing, especially for the compositionally graded transition section. Microstructural characterization revealed unique morphology in each section. Specifically, coarse equiaxed grains were found at the SS 316 substrate. Both acicular and fine equiaxed γ-austenite cells with intercellular δ-ferrite were obtained in pure SS 316L section. Dendritic microstructures were formed at the compositionally transition section. In the pure Al12Si section, Si particles were embedded in the Al matrix. Both cooling rate and compositional variation caused microstructural variations. The EDS mapping demonstrated compositional gradience at the interface between pure SS 316L and pure Al12Si sections. The XRD results showed that FeAl, Fe_2Al_5, and $FeAl_3$ intermetallic phases were formed at the compositionally graded section. After heat treatment, diffused Fe_xAl_y intermetallic phases were obtained near the Fe rich side of the compositionally graded section. None of the silicide phases were obtained from the XRD results. For the non-HT SS 316L/Al12Si sample, microhardness profiles showed the hardness values of SS 316 substrate was 197.1 ± 2.1 $HV_{0.1}$. The DED processed pure SS316L section had a hardness value of 237.8 ± 9.2 $HV_{0.1}$. The hardness was increased to 834.2 ± 107.1 $HV_{0.1}$ at the compositionally graded transition section. The increase in hardness was mainly due to the Fe-Al intermetallic phase formation. The hardness at the pure Al12Si section was 63.2 ± 6.2 $HV_{0.1}$. Similar hardness values were obtained in SS 316L substrate, pure SS 316L, and pure Al12Si sections of HT SS 316L/Al12Si sample compared to non-HT SS 316L/Al12Si sample. However, the hardness at the compositionally graded transition

section of HT SS 316L/Al12Si sample was 578.7 ± 154.1 $HV_{0.1}$, which was ~30% lower compared to the hardness of the non-HT sample at this region. The reduction of hardness was caused due to Fe dominated Fe_xAl_y intermetallic phases formed during the heat treatment. Based on compression test results, the non-HT SS 316L/Al12Si sample's maximum compressive strength was 299.4 ± 22.1 MPa. This value is similar to the HT SS 316L/Al12Si sample's maximum compressive strength, which was 270.1 ± 27.1 MPa. Our results indicate that optimized DED processing parameters can make functional bimetallic SS316L to Al12Si parts.

Acknowledgments

The authors acknowledge financial support from the National Science Foundation under grant # CMMI 1934230 (PI- Bandyopadhyay). Authors also acknowledge financial support from the National Institute of Arthritis and Musculoskeletal and Skin Diseases of the National Institutes of Health under Award Number R01 AR067306. The content is solely the authors' responsibility and does not necessarily represent the official views of the National Institutes of Health. The authors would also like to acknowledge financial support from the JCDREAM (WA) for financial support towards purchasing metal additive manufacturing machines at WSU. The authors would like to acknowledge support from Professor Thomas Williams from the University of Idaho for assistance with XRD analysis.

Data availability

The data that support the findings of this study are available from the corresponding author on reasonable request.

Declaration of Competing Interest

All authors declare that they have no competing interests for this publication.

References

[1] E. Taban, J.E. Gould, J.C. Lippold, Dissimilar friction welding of 6061-T6 aluminum and AISI 1018 steel: Properties and microstructural characterization, Mater. Des. 31 (2010) 2305–2311. https://doi.org/10.1016/j.matdes.2009.12.010.

[2] W. Jiang, Z. Fan, C. Li, Improved steel/aluminum bonding in bimetallic castings by a compound casting process, J. Mater. Process. Technol. 226 (2015) 25–31. https://doi.org/10.1016/j.jmatprotec.2015.06.032.

[3] J.R. Davis, Metals Handbook, 10th. Ed, American Society for Metals, Metals Park, Ohio, 1998. https://doi.org/10.1017/CBO9781107415324.004.

[4] M. Habibnia, M. Shakeri, S. Nourouzi, M.K.B. Givi, Microstructural and mechanical properties of friction stir welded 5050 Al alloy and 304 stainless steel plates, Int. J. Adv. Manuf. Technol. 76 (2014) 819–829. https://doi.org/10.1007/s00170-014-6306-5.

[5] F.A. Besler, P. Schindele, R.J. Grant, M.J.R. Stegmüller, Friction crush welding of aluminium, copper and steel sheetmetals with flanged edges, J. Mater. Process. Technol. 234 (2016) 72–83. https://doi.org/10.1016/j.jmatprotec.2016.03.012.

[6] F.A. Besler, R.J. Grant, P. Schindele, M.J.R. Stegmüller, Advanced Process Possibilities in Friction Crush Welding of Aluminum, Steel, and Copper by Using an Additional Wire, Metall. Mater. Trans. B Process Metall. Mater. Process. Sci. 48 (2017) 2930–2948. https://doi.org/10.1007/s11663-017-1108-4.

[7] L.H. Shah, Z. Akhtar, M. Ishak, Investigation of aluminum-stainless steel dissimilar weld quality using different filler metals, Int. J. Automot. Mech. Eng. 8 (2013) 1121–1131. https://doi.org/10.15282/ijame.8.2013.3.0091.

[8] Y. Liu, X. Bian, J. Yang, K. Zhang, L. Feng, C. Yang, An investigation of metallurgical bonding in Al-7Si/gray iron bimetal composites, J. Mater. Res. 28 (2013) 3190–3198. https://doi.org/10.1557/jmr.2013.328.

[9] S. Kobayashi, T. Yakou, Control of intermetallic compound layers at interface between steel and aluminum by diffusion-treatment, Mater. Sci. Eng. A. 338 (2002) 44–53. https://doi.org/10.1016/S0921-5093(02)00053-9.

[10] S. Yin, X. Yan, C. Chen, R. Jenkins, M. Liu, R. Lupoi, Hybrid additive manufacturing of Al-Ti6Al4V functionally graded materials with selective laser melting and cold spraying, J. Mater. Process. Technol. 255 (2018) 650–655. https://doi.org/10.1016/j.jmatprotec.2018.01.015.

[11] Y. Zhang, A. Bandyopadhyay, Direct fabrication of bimetallic Ti6Al4V+Al12Si structures via additive manufacturing, Addit. Manuf. 29 (2019) 100783. https://doi.org/10.1016/j.addma.2019.100783.

[12] B. Onuike, A. Bandyopadhyay, Additive manufacturing of Inconel 718 – Ti6Al4V bimetallic structures, Addit. Manuf. 22 (2018) 844–851. https://doi.org/10.1016/j.addma.2018.06.025.

[13] B. Onuike, B. Heer, A. Bandyopadhyay, Additive manufacturing of Inconel 718—Copper alloy bimetallic structure using laser engineered net shaping (LENS^{TM}), Addit. Manuf. 21 (2018) 133–140. https://doi.org/10.1016/j.addma.2018.02.007.

[14] B. Onuike, A. Bandyopadhyay, Functional bimetallic joints of Ti6Al4V to SS410, Addit. Manuf. 31 (2020) 100931. https://doi.org/10.1016/j.addma.2019.100931.

[15] H. Sahasrabudhe, R. Harrison, C. Carpenter, A. Bandyopadhyay, Stainless steel to titanium bimetallic structure using LENS^{TM}, Addit. Manuf. 5 (2015) 1–8. https://doi.org/10.1016/j.addma.2014.10.002.

[16] MRU. Ahsan, A.N.M. Tanvir, G.J. Seo, B. Bates, W. Hawkins, C. Lee, P.K. Liaw, M. Noakes, A. Nycz, D.B. Kim, Heat-treatment effects on a bimetallic additively-manufactured structure (BAMS) of the low-carbon steel and austenitic-stainless steel, Addit. Manuf. 32 (2020) 101036. https://doi.org/10.1016/j.addma.2020.101036.

[17] L. Liu, Z. Zhuang, F. Liu, M. Zhu, Additive manufacturing of steel-bronze bimetal by shaped metal deposition: Interface characteristics and tensile properties, Int. J. Adv. Manuf. Technol. 69 (2013) 2131–2137. https://doi.org/10.1007/s00170-013-5191-7.

[18] D. Kono, A. Maruhashi, I. Yamaji, Y. Oda, M. Mori, Effects of cladding path on workpiece geometry and impact toughness in Directed Energy Deposition of 316L stainless steel, CIRP Ann. 67 (2018) 233–236. https://doi.org/10.1016/j.cirp.2018.04.087.

[19] DR Eo, S.H. Park, J.W. Cho, Inclusion evolution in additive manufactured 316L stainless steel by laser metal deposition process, Mater. Des. 155 (2018) 212–219. https://doi.org/10.1016/j.matdes.2018.06.001.

[20] J. Yu, M. Rombouts, G. Maes, Cracking behavior and mechanical properties of austenitic stainless steel parts produced by laser metal deposition, Mater. Des. 45 (2013) 228–235. https://doi.org/10.1016/j.matdes.2012.08.078.

[21] MJK. Lodhi, K.M. Deen, W. Haider, Corrosion behavior of additively manufactured 316L stainless steel in acidic media, Materialia. 2 (2018) 111–121. https://doi.org/10.1016/j.mtla.2018.06.015.

[22] J. Li, X. Cheng, Z. Li, X. Zong, S.Q. Zhang, H.M. Wang, Improving the mechanical properties of Al-5Si-1Cu-Mg aluminum alloy produced by laser additive manufacturing with post-process heat treatments, Mater. Sci. Eng. A. (2018). https://doi.org/10.1016/j.msea.2018.08.074.

[23] J. Li, X. Cheng, Z. Li, X. Zong, X.H. Chen, S.Q. Zhang, H.M. Wang, Microstructures and mechanical properties of laser additive manufactured Al-5Si-1Cu-Mg alloy with different layer thicknesses, J. Alloys Compd. 789 (2019) 15–24. https://doi.org/10.1016/j.jallcom.2019.03.101.

[24] T. Tarasova, G. Gvozdeva, R. Ableyeva, Aluminium Matrix Composites Produced by Laser-Based Additive Manufacturing, Mater. Today Proc. 11 (2019) 305–310. https://doi.org/10.1016/j.matpr.2018.12.149.

[25] A. Simchi, The role of particle size on the laser sintering of iron powder, Metall. Mater. Trans. B Process Metall. Mater. Process. Sci. 35 (2004) 937–948. https://doi.org/10.1007/s11663-004-0088-3.

[26] B. Zheng, J.C. Haley, N. Yang, J. Yee, K.W. Terrassa, Y. Zhou, E.J. Lavernia, J.M. Schoenung, On the evolution of microstructure and defect control in 316L SS components fabricated via directed energy deposition, Mater. Sci. Eng. A. 764 (2019) 138243. https://doi.org/10.1016/j.msea.2019.138243.

[27] M. H. Farshidianfar, A. Khajepour, A.P. Gerlich, Effect of real-time cooling rate on microstructure in Laser Additive Manufacturing, J. Mater. Process. Technol. 231 (2016) 468–478. https://doi.org/10.1016/j.jmatprotec.2016.01.017.

[28] MJK. Lodhi, K.M. Deen, M.C. Greenlee-Wacker, W. Haider, Additively manufactured 316L stainless steel with improved corrosion resistance and biological response for biomedical applications, Addit. Manuf. 27 (2019) 8–19. https://doi.org/10.1016/j.addma.2019.02.005.

[29] Y. Huang, M. Ansari, H. Asgari, M.H. Farshidianfar, D. Sarker, M.B. Khamesee, E. Toyserkani, Rapid prediction of real-time thermal characteristics, solidification parameters, and microstructure in laser directed energy deposition (powder-fed additive manufacturing), J. Mater. Process. Technol. 274 (2019). https://doi.org/10.1016/j.jmatprotec.2019.116286.

[30] W. Hofmeister, M. Griffith, M. Ensz, J. Smugeresky, Solidification in direct metal deposition by LENS processing, Jom. 53 (2001) 30–34. https://doi.org/10.1007/s11837-001-0066-z.

[31] W. J. Yuan, R. Li, Q. Shen, L.M. Zhang, Characterization of the evaluation of the solid solubility of Si in sintered Fe-Si alloys using DSC technique, Mater. Charact. 58 (2007) 376–379. https://doi.org/10.1016/j.matchar.2006.06.003.

[32] J. L. Murray, Fe–Al binary phase diagram, Alloy Phas, ASM International, Materials Park, OH, 1992.

[33] L. Tricarico, R. Spina, D. Sorgente, M. Brandizzi, Effects of heat treatments on mechanical properties of Fe/Al explosion-welded structural transition joints, Mater. Des. 30 (2009) 2693–2700. https://doi.org/10.1016/j.matdes.2008.10.010.

[34] ASTM E9-09, Standard Test Methods of Compression Testing of Metallic Materials at Room Temperature, (2009).

[35] S. Scari, BC. Pockszevnicki, J.L. Junior, P. Americo, A. Magalhaes, Stress-Strain Compression of AA6082-T6 Aluminum Alloy at Room Temperature, J. Struct. 2014 (2014) 7.

[36] NE. Dowling, Mechanical Behavior of Materials Engineering Methods for Deformation, Fracture, and Fatigue, Pearson Educ. (2013) 1–30.

[37] H. N. Han, K.H. Kim, A ductile fracture criterion in sheet metal forming process, J. Mater. Process. Technol. 142 (2003) 231–238.

[38] Z. Shi, J. Cao, F. Han, Preparation and characterization of Fe-Al intermetallic layer on the surface of T91 heat-resistant steel, J. Nucl. Mater. 447 (2014) 77–81. https://doi.org/10.1016/j.jnucmat.2013.12.027.

[39] A. da S. Scari, BC. Pockszevnicki, J. Landre Junior, P.A.A. Magalhaes Junior, Stress-Strain Compression of AA6082-T6 Aluminum Alloy at Room Temperature, J. Struct. 2014 (2014) 1–7. https://doi.org/10.1155/2014/387680.

Supplementary document

Tailoring compositionally graded interface of 316L stainless steel to Al12Si aluminum alloy bimetallic structures via Additive Manufacturing

Yanning Zhang and Amit Bandyopadhyay*

School of Mechanical and Materials Engineering

Washington State University

Pullman, WA 99164-2920, USA.

*Corresponding author's E-mail: amitband@wsu.edu

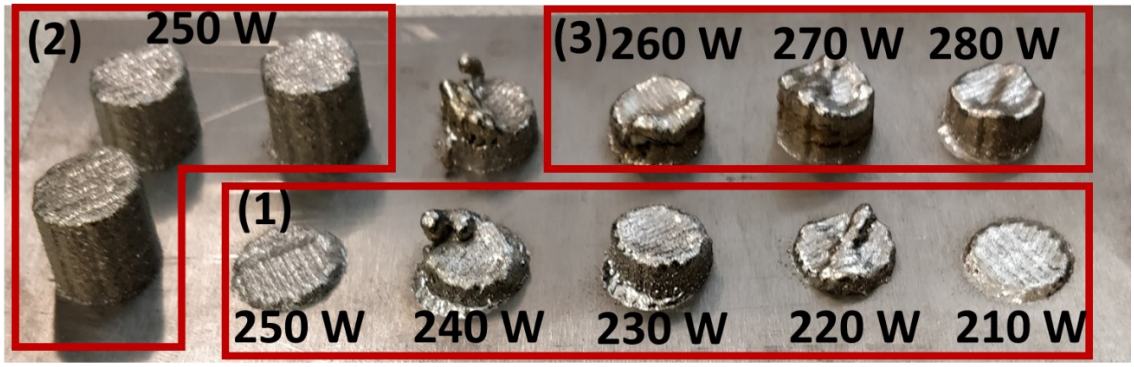

Figure S1. DED processing parameters optimization of pure SS 316L. The designed cylindrical structure had a 0.5-inch diameter and 1-inch height. All samples were fabricated using a hatch distance of 0.417 mm, a constant laser scan speed of 1200 mm/s, and a layer thickness of 0.15 mm. Group 1 was fabricated by a laser power of 210-250 W. Based on the results of the as-fabricated layer, using 250 W to fabricate, SS 316L showed the best result. Group 2 were the cylindrical SS 316L structures fabricated by 250 W. The dimension of the parts from group 2 was closed to the design. Group 3 was fabricated by utilizing laser power from 260 W to 280 W. These parts had a concave top surface, and the as-fabricated parts could not reach 1-inch height, which was caused by high laser power.

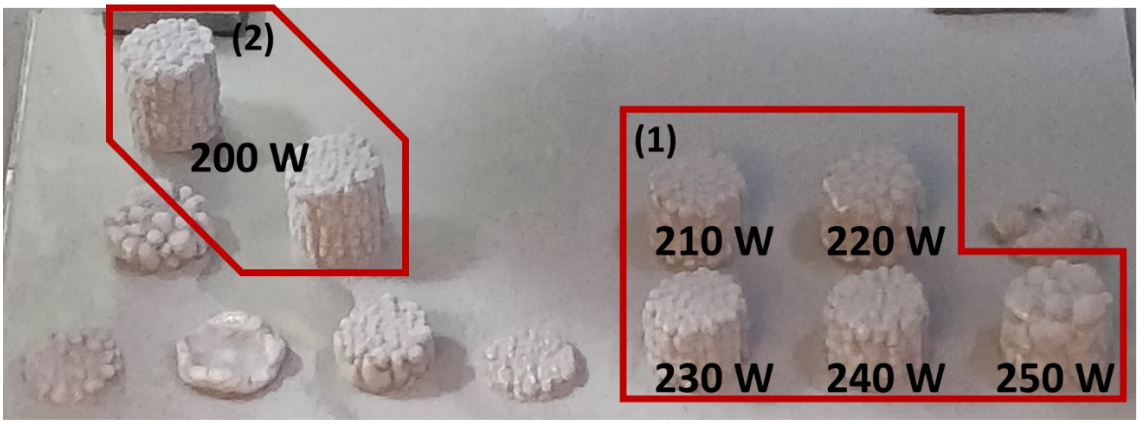

Figure S2. DED processing parameters optimization of pure Al12Si. The designed cylindrical structure had a 0.5-inch diameter and 1-inch height. All samples were fabricated using a hatch distance of 0.417 mm, a constant laser scan speed of 1200 mm/s, and a layer thickness of 0.25 mm. Group 1 was fabricated by using laser power from 250 W – 210 W. The sample fabricated with 250 W formed a large "bubble" around the surface and could hardly form a cylindrical structure. With laser power reduction, the "bubble" became smaller, and samples could form near cylindrical shape. However, the as-fabricated samples could not reach a 1-inch height. Group 2 was fabricated with 200 W laser power. The final dimension of samples from group 2 was closed to design with no defects.

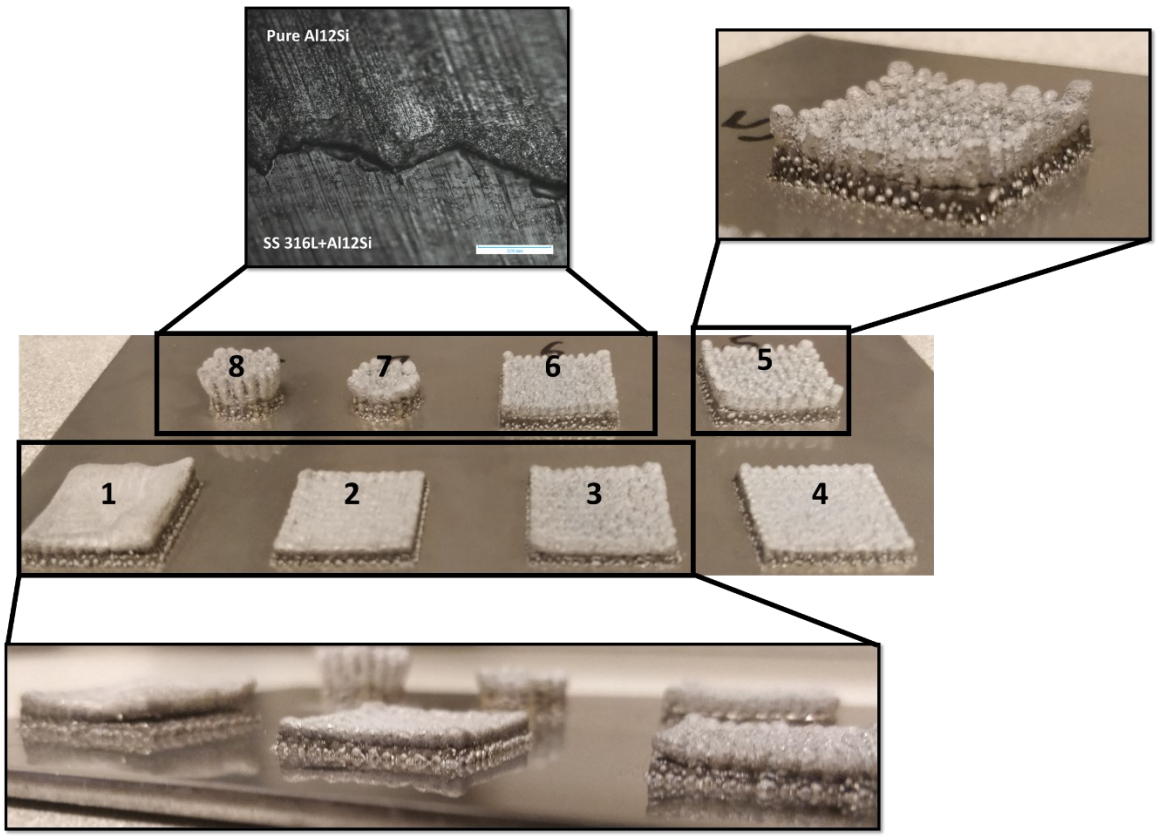

Figure S3. Sample 1-8 were the DED fabricated SS 316L/Al12Si bimetallic structures using a constant SS 316L-rich SS 316L+Al12Si mixed composition as transition section (powder feed rate of SS 316L and Al12Si were 18.4 g/min and 1.3 g/min). For each sample, the number of transition layers varies. Specifically, samples 1, 2, and 3 had several transition layers of 8, 7, and 6. Based on the results, sample 1 had delamination in the transition section. Sample 2 and 3 had cracks at the interface between the mixed section and pure Al12Si section. Sample 4 and 5 had 5 layers of mixed composition. The result showed that horizontal cracks could also be found on these samples. Sample 6, 7, and 8 had 4 layers of mixed composition. Although no visible defects could be seen on these samples, however, according to the microscope analysis, a horizontal gap was found at the interface between the SS 316L+Al12Si section and pure Al12Si, which indicated poor bonding.

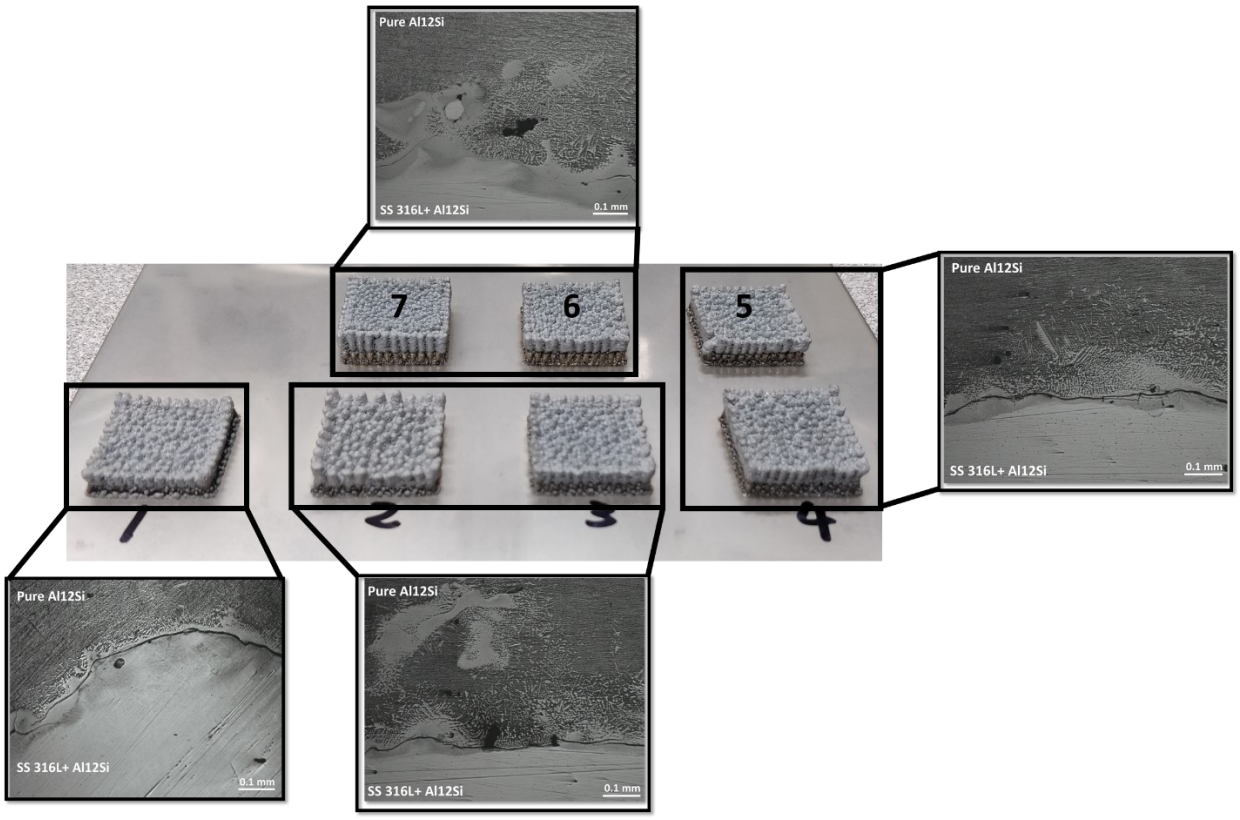

Figure S4. Sample 1-8 were the DED fabricated SS 316L/Al12Si bimetallic structures using a constant Al12Si-rich SS 316L+Al12Si mixed composition as transition section (powder feed rate of SS 316L and Al12Si were 3 g/min and 8.4 g/min). Each sample had a different number of the transition layer. Specifically, sample 1 had 7 layers of mixed composition. Sample 2 and 3 had 6 transition layers. Sample 4 and 5 had 5 transition layers. Sample 6 and 7 had 4 transition layers. No visible defects were found on all these samples. However, based on the microscope analysis, samples 7 and 8 had minimum cracks at the interface between the SS 316L+Al12Si section and pure Al12Si section.